MODEL-BASED CONTROL OF CARDIAC ALTERNANS IN A MODEL OF PURKINJE FIBERS

Alejandro Garzón
Department of Sciences
Fundación Universitaria Agraria de Colombia
Colombia
agarzon75@gmail.com

Roman O. Grigoriev
School of Physics
Georgia Institute of Technology
United States
romgrig@gatech.edu

Abstract

This paper describes a systematic approach to suppressing cardiac alternans in Purkinje fibers using localized current injections. We investigate the controllability and observability of the periodically paced Noble model for different locations of the recording and control electrodes. In particular, we show that the loss of controllability causes the failure of the control approach introduced by Echebarria and Karma [*Chaos* **12**, 923 (2002)] for longer fiber lengths. Furthermore, we explain how the optimal locations for the recording and control electrodes and the timing of the feedback current can be selected, accounting for both linear and nonlinear effects, effectively doubling the length of fibers that can be controlled.

Key words

Cardiac dynamics, alternans, feedback control

1 Introduction

When excitable cardiac tissue is electrically paced at a sufficiently high rate, the duration of excitation (or action potential duration, APD) can alternate from beat to beat [Mines, 1913] despite a fixed stimulation period. This rhythm, known as alternans or 2:2, has been identified [Pastore *et al.*, 1999; Watanabe *et al.*, 2001] as an early stage in a sequence of increasingly complex instabilities leading to the lethal type of arrhythmia known as ventricular fibrillation (VF) [Cherry and Fenton, 2008]. Hence, suppression of alternans can be considered as a way of mitigating VF.

In this paper we focus on control of alternans in a specific type of cardiac tissue, Purkinje fibers, which conducts the electrical excitation from the atria to the ventricles. Echebarria and Karma [Echebarria and Karma, 2002] were the first to investigate suppression of alternans in a model of Purkinje fibers by adjusting the pacing interval based on the difference between the two most recent APDs. Their approach, referred to as the pacing interval adjustment (PIA) method here, is a particular implementation of the empiric delayed feedback control of Pyragas [Pyragas, 1992]. The earliest implementation of Pyragas' approach to cardiac tissue is due to Hall and Gauthier who managed to suppress alternans in small patches of frog heart muscle tissue [Hall and Gauthier, 2002]. While PIA control has the benefit that no model of the dynamics is required, it also has limitations: numerical simulations of the Noble model showed that PIA is unable to suppress alternans in fibers longer than about 1 cm [Echebarria and Karma, 2002]. This theoretic prediction was verified experimentally by Christini et al. [Christini *et al.*, 2006]. Studies of other models of cardiac dynamics also find a limit on the fiber length that can be controlled by a single electrode [Rappel *et al.*, 1999] using a non-model-based approach.

This limitation relates many factors, such as the number and location of electrodes used for control as well as the law used to compute the feedback current. This paper presents the analysis of these factors. To enable direct comparison with the results of Ref. [Echebarria and Karma, 2002], we consider a configuration with one electrode recording the transmembrane potential and one control electrode (not necessarily collocated) applying the feedback current in the form of one well localized pulse per pacing interval. We also use the Noble model [Noble, 1962] for the ion channel dynamics

$$\partial_t \mathbf{z} = D\partial_x^2 \mathbf{z} + F(\mathbf{z}) - I_p \mathbf{g}(x_p) - I_c \mathbf{g}(x_c), \qquad (1)$$

where $\mathbf{z}(x,t) = [u, a, b, c]$ is the vector of cellular state variables: the scaled transmembrane voltage u and the gating variables a, b, and c of the local ionic model $F(\mathbf{z})$. D is a 4×4 matrix whose only nonzero element D_{11} describes electric coupling between cells. All parameter values are chosen as in Ref. [Echebarria and Karma, 2002]. While not the most accurate model of Purkinje fibers, the Noble model captures the essential dynamics and provides an opportunity for direct com-

parison of our results with previous studies.

The last two terms in (1) describe the pacing and feedback currents $I_p(t)$ and $I_c(t)$, while $\mathbf{g}(x_i) \equiv [g(x - x_i), 0, 0, 0]$, where $g(x - x_i)$ is the spatial distribution of the current density applied by an electrode centered at x_i, which we take to be a normalized Gaussian with width $\sigma = 0.1$ cm. Although it can be argued that control may be more effective when applied to one of the gating variables (i.e., a, b, or c here) [Muñoz *et al.*, 2010], in practice it is much easier to control the current, so this is the approach we pursue here. The location of the pacing electrode in this study is $x_p = 0.25$ cm, while the location of the control electrode x_c is to be chosen later. No-flux boundary conditions are imposed at both ends of the fiber, $\partial_x u|_{x=0,L} = 0$.

The model (1) with $I_c(t) = 0$ possesses a time-periodic solution $\mathbf{z}_0(t)$, corresponding to a normal rhythm with a 1:1 response, with the period T determined by the pacing current $I_p(t) = I_p^0(t \mod T)$, where

$$I_p^0(t) = \begin{cases} I_0, \ 0 < t < \Delta T_p, \\ 0, \ \Delta T_p < t < T, \end{cases} \tag{2}$$

and the pulse duration ΔT_p was chosen equal to 5 ms. As is well known [Guevara *et al.*, 1984], this rhythm is linearly stable for slow pacing rates. For faster pacing it becomes unstable and is replaced by a limit cycle oscillation which corresponds to the state of alternans. The goal of control is to suppress the transition to alternans by extending the linear stability of the normal rhythm to shorter T. This can be achieved by monitoring the transmembrane voltage using a recording electrode at x_o and applying an appropriately chosen feedback current $I_c(t)$ through the control electrode. In particular, in PIA the recording and control electrodes are collocated with the pacing electrode ($x_o = x_c = x_p$), and the pacing period becomes a function of the action potential duration APD_n following the n^{th} pacing impulse, $T^n = T + \Delta T^n$, with

$$\Delta T^n = \gamma(\mathrm{APD}_n - \mathrm{APD}_{n-1})/2, \tag{3}$$

which corresponds to $I_c(t) = I_p(t - T - \Delta T^n) - I_p(t - T)$.

Consider the dynamics of small perturbations $\delta\mathbf{z} = \mathbf{z} - \mathbf{z}_0$ about the target state $\mathbf{z}_0$, governed by the linearization of (1)

$$\partial_t \delta\mathbf{z} = D\partial_x^2 \delta\mathbf{z} + J\delta\mathbf{z} - I_c\mathbf{g}(x_c), \tag{4}$$

where $J(t) \equiv DF/D\mathbf{z}|_{\mathbf{z}_0(t)}$ is the Jacobian of $F(\mathbf{z})$ evaluated along the periodic orbit $\mathbf{z}_0(t)$. Introducing the stroboscopic section $t_n = \tau + nT$, the evolution can be recast in terms of a map which, in the absence of control, has the form

$$\delta\mathbf{z}(t_{n+1}) = U(\tau + T, \tau)\delta\mathbf{z}(t_n), \tag{5}$$

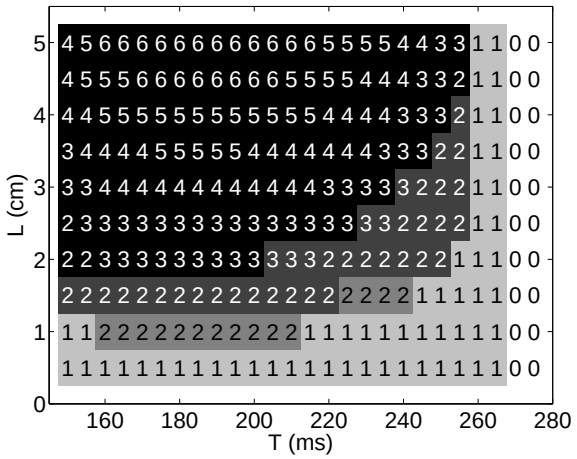

Figure 1. Stability diagram, showing the number of unstable modes for normal rhythm. White indicates the region in parameter space where normal rhythm is stable. Alternans can be successfully suppressed using PIA control only in the light gray region. Model-based control is successful everywhere in the gray shaded regions. Feedback is computed using the complete system state in the dark gray region or using local voltage recordings in the medium and light gray regions. All control methods we investigated fail in the black region.

where $U(t_f, t_i)$ denotes the time evolution operator of (4) for the time interval (t_i, t_f) and $\tau = 0$ defines the timing of the pacing impulse. The stability of $\mathbf{z}_0$ is determined by the eigenvalues λ_i of the map (5). Here we assume $|\lambda_1| \geq |\lambda_2| \geq \cdots$. It can be shown that λ_i are independent of τ and that the eigenmodes of $U(\tau + T, \tau)$ for arbitrary τ can be computed as $\mathbf{e}_i(\tau) = U(\tau, 0)\mathbf{e}_i(0)$ using the eigenmodes for $\tau = 0$.

The periodic solution $\mathbf{z}_0(t)$ is found using a combination of a matrix-free Newton-Krylov method [Knoll and Keyes, 2004] and generalized minimal residual method (GMRES). The latter is implemented by the MATLAB (Mathworks, Inc.) routine **gmres**. The spectrum of $U(T, 0)$ is then found using the implicitly re-started Arnoldi iteration method [Lehoucq and Sorensen, 1996], implemented by the MATLAB routine **eigs**. For the sake of efficiency, this method was also applied in its matrix-free form using a routine that calculates the matrix-vector product, in this case $U(T, 0)\delta\mathbf{z}$, instead of the explicit matrix representation of $U(T, 0)$. The matrix-free method is based on numerical integration of (1) using the explicit Euler method and finite differences with $\Delta x = 0.01$ cm and $\Delta t = 0.01$ ms. The number of unstable eigenvalues ($|\lambda_i| > 1$) found for a grid of pairs (L, T) is shown in Fig. 1. We find that, for the range of L values considered, the normal rhythm $\mathbf{z}_0(t)$ becomes unstable at nearly the same period ($T \approx 270$ ms) and alternans develops, which is consistent with Ref. [Echebarria and Karma, 2002].

2 Controllability

In the presence of feedback Eq. (5) must be modified. For simplicity we assume the feedback current is

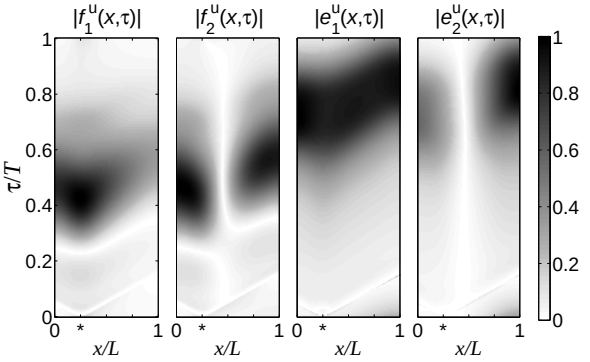

Figure 2. Controllability and observability of the two unstable modes for $L = 1$ cm and $T = 210$ ms. The star indicates the location of the pacing electrode. The grayscale shows the magnitude of the indicated eigenmodes. The mode structure is similar for other values of L and T.

applied during a brief time interval $(t_n, t_n + \delta t)$. For $\delta t \ll T$,

$$\delta\mathbf{z}(t_n + \delta t) \approx \delta\mathbf{z}(t_n) - Q^n\mathbf{g}(x_c), \tag{6}$$

where Q^n is the total electric charge delivered by the control electrode during that interval. Hence the stroboscopic map becomes

$$\delta\mathbf{z}(t_{n+1}) = U(\tau + T, \tau)\delta\mathbf{z}(t_n) - Q^n\mathbf{b}, \tag{7}$$

where $\mathbf{b} = U(\tau + T, \tau)\mathbf{g}(x_c)$. A more convenient description of the dynamics can be obtained by projecting (7) onto the basis $\{\mathbf{e}_i(\tau)\}$. This requires the eigenmodes $\mathbf{f}_i(\tau)$ of the adjoint evolution operator

$$U^\dagger(\tau + T, \tau)\mathbf{f}_i(\tau) = \lambda_i^*\mathbf{f}_i(\tau). \tag{8}$$

The adjoint eigenmodes $\mathbf{f}_i(0)$ are computed using the matrix-free approach described previously. The action of the operator $U^\dagger(t, 0)$ is computed by time-discretizing $U(t, 0)$ and evaluating the adjoint of the resulting composition of operators. The relationship $\mathbf{f}_i(\tau) = (\lambda_i^*)^{-1} U^\dagger(T, \tau)\mathbf{f}_i(0)$ is then used to compute the eigenmodes for other values of τ.

When properly normalized, the eigenmodes $\mathbf{e}_i(\tau)$ and $\mathbf{f}_i(\tau)$ satisfy the orthogonality condition

$$\langle\mathbf{f}_i(\tau), \mathbf{e}_i(\tau)\rangle \equiv \int_0^L \mathbf{f}_i^*(\tau) \cdot \mathbf{e}_j(\tau)dx = \delta_{ij}. \tag{9}$$

Therefore, we can expand the perturbation

$$\delta\mathbf{z}(t_n) = \sum_{i=1}^{\infty} \xi_i^n\mathbf{e}_i(\tau), \tag{10}$$

where $\xi_i^n = \langle\mathbf{f}_i(\tau), \delta\mathbf{z}(t_n)\rangle$. Applying the operation $\langle\mathbf{f}_i(\tau), \cdot\rangle$ to both sides of (7) we obtain

$$\xi_i^{n+1} = \lambda_i\xi_i^n - B_iQ^n, \tag{11}$$

where $B_i = \langle\mathbf{f}_i(\tau), \mathbf{b}\rangle = \lambda_i \langle\mathbf{f}_i(\tau), \mathbf{g}(x_c)\rangle \approx \lambda_i f_i^u(x_c, \tau)$, since $g(x)$ is a narrow Gaussian (the superscript u denotes the voltage component of $\mathbf{f}_i$).

In the limit $\Delta T^n \ll \Delta T_p \ll T$, which corresponds to small deviations from normal rhythm, PIA control can be cast in a form very similar to (11):

$$\xi_i^{n+1} \approx \lambda_i\xi_i^n - \lambda_i [f_i^u(x_p, \Delta T_p) - f_i^u(x_p, 0)]\frac{Q_p}{\Delta T_p}\Delta T^n, \tag{12}$$

where Q_p is the charge delivered by one pacing impulse of duration ΔT_p and ΔT^n was defined in (3).

When $f_i^u(x_c, \tau) \approx 0$ for some i, the feedback current has no effect on the dynamics of mode i (the mode becomes *uncontrollable*) and the instability cannot be suppressed, regardless of how the current is chosen. On the other hand, the larger $|f_i^u(x_c, \tau)|$ is, the smaller the feedback current can be. The structure of the adjoint eigenmodes, therefore, determines where the control electrode(s) should be placed and how the timing of the control impulse should be chosen. Similar conclusion was made for spiral waves in a two-dimensional tissue model in Ref. [Allexandre and Otani, 2004].

Fig. 2 shows the absolute value of the adjoint eigenmodes for the two unstable modes of our system. Using the same electrode for both pacing and control is not only convenient from the experimental perspective, this choice also provides near optimal controllability. As Fig. 2 illustrates, $|f_i^u(x_p, \tau)|$ reaches near-maximal values for all unstable modes, such that they can be made controllable by appropriate choice of τ. Therefore, in this study we set $x_c = x_p$. Controllability also requires that the control impulse be delivered much later than the pacing impulse. We discovered that the optimal interval $0.3T \lesssim \tau \lesssim 0.6T$, where $|f_i^u(x_p, \tau)|$ takes nearly maximal values for all unstable modes (hence requiring the smallest control current), is essentially independent of L. As Fig. 4 shows, this corresponds to the plateau phase of the action potential. However, as we will see next, there may be other conditions that impose additional restrictions on the choice of τ.

For PIA, feedback timing does not fall into the optimal range. On the contrary, for every i, $|f_i^u(x_p, \tau)|$ has a deep minimum in the range $0 < \tau < \Delta T_p$, as Fig. 3 shows. As the right-hand-side of (12) shows, when feedback is imposed by shifting the timing of the pacing impulse, the magnitude of the difference $\Delta f_i^u \equiv f_i^u(x_p, \Delta T_p) - f_i^u(x_p, 0)$ determines controllability instead of $|f_i^u(x_p, \tau)|$. As Table 1 shows, $|\Delta f_i^u|$ is of order unity only for $i = 1$ (the leading

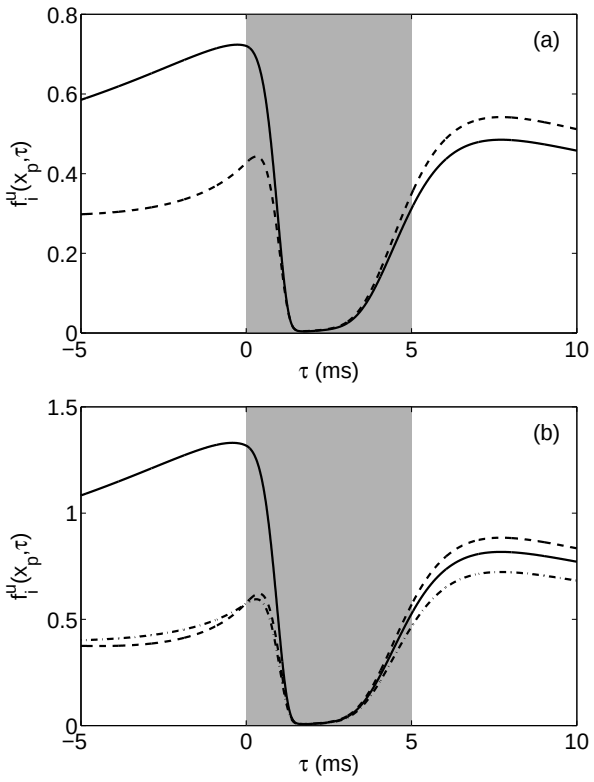

Figure 3. $f_i^u(x_p, \tau)$ for (a) $L = 1$ cm and (b) $L = 2$ cm. In both cases $T = 210$ ms. Only i-values for unstable modes are shown: $i = 1$ (solid line), $i = 2$ (dashed line), $i = 3$ (dot-dashed line). The gray shade indicates the range $0 < \tau < \Delta T_p$.

mode is controllable). All sub-leading modes are, at best, weakly controllable, indicating that PIA control has virtually no effect on their dynamics and hence is expected to fail. This is in perfect agreement with Ref. [Echebarria and Karma, 2002], which showed that feedback only affects the dynamics of the leading mode.

Once x_c and τ have been selected, the feedback stabilizing the target state can be computed using any standard control-theoretic method. We start by truncating (11), keeping only the unstable and possibly some weakly stable modes. The evolution equation for the m remaining modes can be written in matrix form as $\xi^{n+1} = A\xi^n - BQ^n$, where $\xi^n = [\xi_1^n, \cdots, \xi_m^n]$, A is a diagonal matrix with $A_{ii} = \lambda_i$, and $B = [B_1, \cdots, B_m]$. We compute the stabilizing feedback using linear-quadratic regulator control (using MAT-

i	1	2	3	4
$\lvert\Delta f_i^u\rvert^{(a)}$	**0.4080**	**0.0780**	0.0054	0.0926
$\lvert\Delta f_i^u\rvert^{(b)}$	**0.7909**	**0.0082**	**0.1086**	0.0716

Table 1. The values of $|\Delta f_i^u| = |f_i^u(x_p, \Delta T_p) - f_i^u(x_p, 0)|$ for (a) $L = 1$ cm and (b) $L = 2$ cm. Bold font corresponds to unstable modes. In both cases $T = 210$ ms.

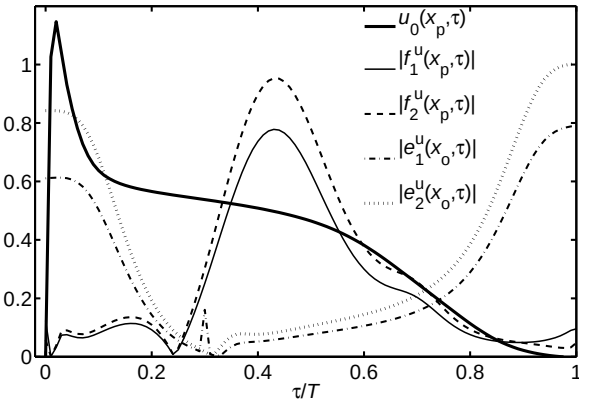

Figure 4. Controllability and observability of the unstable modes and sinus rhythm voltage for $L = 2$ cm, $T = 220$ ms, $x_c = x_p = 0.25$ cm and $x_o = 1.8$ cm.

LAB routine **dlqr**) which yields

$$Q^n = -K\xi^n, \tag{13}$$

with feedback gain K making $A + BK$ stable.

3 Stabilizability

In experiment, the mode amplitudes ξ_i^n will not be directly accessible. However, it is possible to reconstruct them from recordings of the transmembrane voltage using an auxiliary dynamical system known in control theory as an *observer* or *estimator*. Similar to the PIA implementation in Ref. [Echebarria and Karma, 2002], we will use a single electrode to record the voltage, but will use one measurement per pacing interval in contrast with PIA, which requires continuous measurement of u to determine the APD. An electrode of finite spatial extent and centered at x_o can be modeled by writing the recorded voltage as $v^n = \int g(x - x_o)u(x, t_n)dx$. We also assume that the voltage in the normal rhythm $v_0 = \int g(x - x_o)u_0(x, \tau)dx$ is unknown and needs to be determined. In principle, τ can be chosen independently for observation and control; in this study we choose τ to be the same for simplicity.

From the definition of $\delta\mathbf{z}$ and (10) we have

$$v^n = v_0 + \sum_{i=1}^{\infty} \xi_i^n C_i, \tag{14}$$

where $C_i = \langle \mathbf{e}_i(\tau), \mathbf{g}(x - x_o)\rangle \approx e_i^u(x_o, \tau)$. Truncating (14) to m modes and rewriting it in matrix form yields $v^n = C^\dagger \mathbf{r}^n$, where $C = [C_1, \cdots, C_m, 1]$ and $\mathbf{r}^n = [\xi_1^n, \cdots, \xi_m^n, v_0]$ is the vector of unknowns to be determined. Once again, (14) allows an intuitive interpretation. Whenever $C_i \approx e_i^u(x_o, \tau) = 0$, the measured voltage becomes independent of the mode amplitude ξ_i^n (mode i becomes *unobservable*). This means that ξ_i^n cannot be determined regardless of the procedure used to extract it. If the unobservable mode is

unstable, we cannot expect the feedback to suppress it either, so that observability of unstable modes imposes additional restrictions on the timing τ of voltage recordings and the position x_o of the recording electrode. From the observability standpoint, the optimal choice of τ corresponds to the range where both $|e_1^u(x_p,\tau)|$ and $|e_2^u(x_p,\tau)|$ are near maximal values. This optimal range is L-dependent: we find $0.5T \lesssim \tau \lesssim 0.9T$ for $L = 1$ cm (see Fig. 2), but $0.8T \lesssim \tau \lesssim 1.2T$ for $L = 2$ cm (see Fig. 4). On the other hand, the optimal spatial location for the recording electrode, regardless of fiber length, is found to be $x_o \approx 0.9L$.

We used the Luenberger observer [Zak, 2003] to reconstruct the mode amplitudes ξ_i^n from a series of voltage recordings $v^n, v^{n-1}, \cdots$. Let us define

$$\tilde{\mathbf{r}}^{n+1} = \widetilde{A}\tilde{\mathbf{r}}^n + \widetilde{B}Q^n + H\left[v^n - C^\dagger \tilde{\mathbf{r}}^n\right], \qquad (15)$$

where $\widetilde{A}$ is a diagonal matrix with $\widetilde{A}_{ii} = \lambda_i$ for $i = 1, \cdots, m$ and $\widetilde{A}_{ii} = 1$ for $i = m+1$, while $\widetilde{B}_i = B_i$ for $i = 1, \cdots, m$ and $\widetilde{B}_i = 0$ for $i = m+1$. Then $\tilde{\mathbf{r}}^n = [\tilde{\xi}_1^n, \cdots, \tilde{\xi}_m^n, \tilde{v}_0]$ is an estimate of $\mathbf{r}^n$ in the sense that the difference $\tilde{\mathbf{r}}^n - \mathbf{r}^n$ converges to zero asymptotically, provided H is chosen such that $\widetilde{A} - HC$ is stable. The observer gain H was also computed using **dlqr**.

Combining the controller (13) with the observer (15) yields a single-input single-output (SISO) control procedure (known as a *compensator*) that could easily be applied in an experimental setting. To illustrate its performance we implemented control of the full nonlinear equation (1).

4 Results and conclusions

In order to directly compare the performance of the compensator with PIA control we used the same electrode for pacing and feedback and followed the protocol outlined in Ref. [Echebarria and Karma, 2002]. Starting with $T = 280$ ms where the normal rhythm is stable, T was decreased by 5 ms followed by 200 pacing impulses (with the feedback turned on) after which the cycle was repeated. We found that, PIA control is able to suppress alternans only for the values of L and T characterized by one unstable mode (see Fig. 1). This result supports the observation we made previously that the second unstable mode becomes uncontrollable whenever the control current is localized near $\tau = T$ (or $\tau = 0$), as is the case for PIA.

The failure of PIA control is illustrated in Fig. 5(a) which shows the evolution of the two unstable modes for $L = 1$ cm. Although initially quite small, the amplitude of the sub-leading mode grows exponentially with the rate close to that predicted by the linear stability analysis in the absence of control, as expected. The leading mode, on the other hand, is controllable and hence is initially suppressed by feedback. However, its dynamics is slaved to that of the growing sub-leading mode through the nonlinear terms in (1). Once the amplitude of the sub-leading mode becomes sufficiently

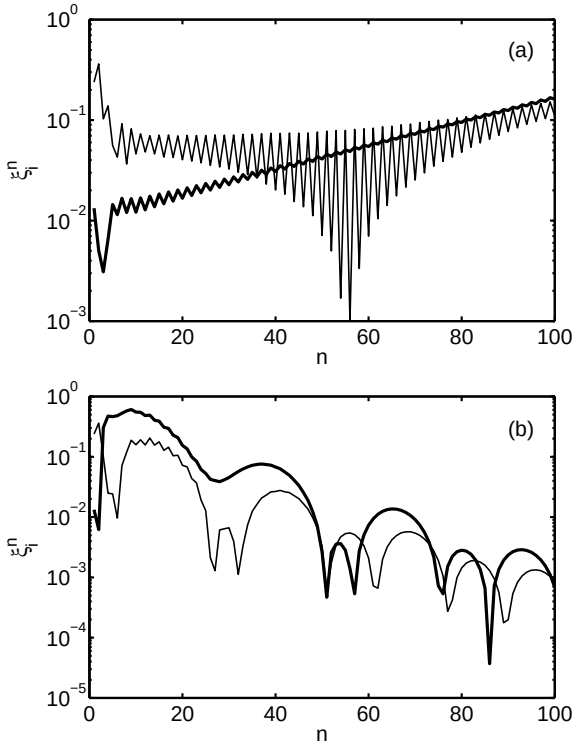

Figure 5. Modal amplitudes ξ_1^n (thin line) and ξ_2^n (thick line) during PIA (a) and model-based control (b) for $L = 1$ cm and $T = 205$ ms. In both cases the initial condition is the normal rhythm for $T = 210$ ms and control is turned on at $n = 1$.

large, the leading mode also starts to grow as feedback is overpowered by mode coupling.

In contrast, the compensator succeeds even when additional unstable modes appear, as Fig. 1 shows. For instance, for $L = 1$ cm, controllability and observability conditions can be satisfied by placing the recording electrode in the optimal location $x_o = 0.9$ cm and choosing $\tau = 0.54T$. In this case truncation to $m = 2$ modes is sufficient to suppress alternans for any T, including the values where PIA control fails, as illustrated by Fig. 5(b). On the other hand, if the pacing electrode is also used for observation, $x_o = x_c = 0.25$ cm, the compensator performance deteriorates significantly when the same 2-mode truncation is used. Predictably, it is the observer part which starts to fail in the latter case. As a quick comparison of Figs. 6(a) and 6(b) shows, for $x_o = 0.25$ cm the estimates of the modal amplitudes differ significantly from the actual values, while for $x_o = 0.9$ cm the estimates remain fairly accurate. The fundamental problem here is the decreased observability of both unstable modes at $x_o = 0.25$ cm (see Fig. 2), which requires the use of a large observer gain H. The latter, in turn, reduces the region of validity of the linear approximation (15). Since the initial condition $\mathbf{z}_i$ (normal rhythm at $T = 210$ ms) deviates quite significantly from the target state $\mathbf{z}_0$ (normal rhythm at $T = 205$ ms), large observer gain can significantly amplify nonlinear effects, artificially exciting nominally stable modes not

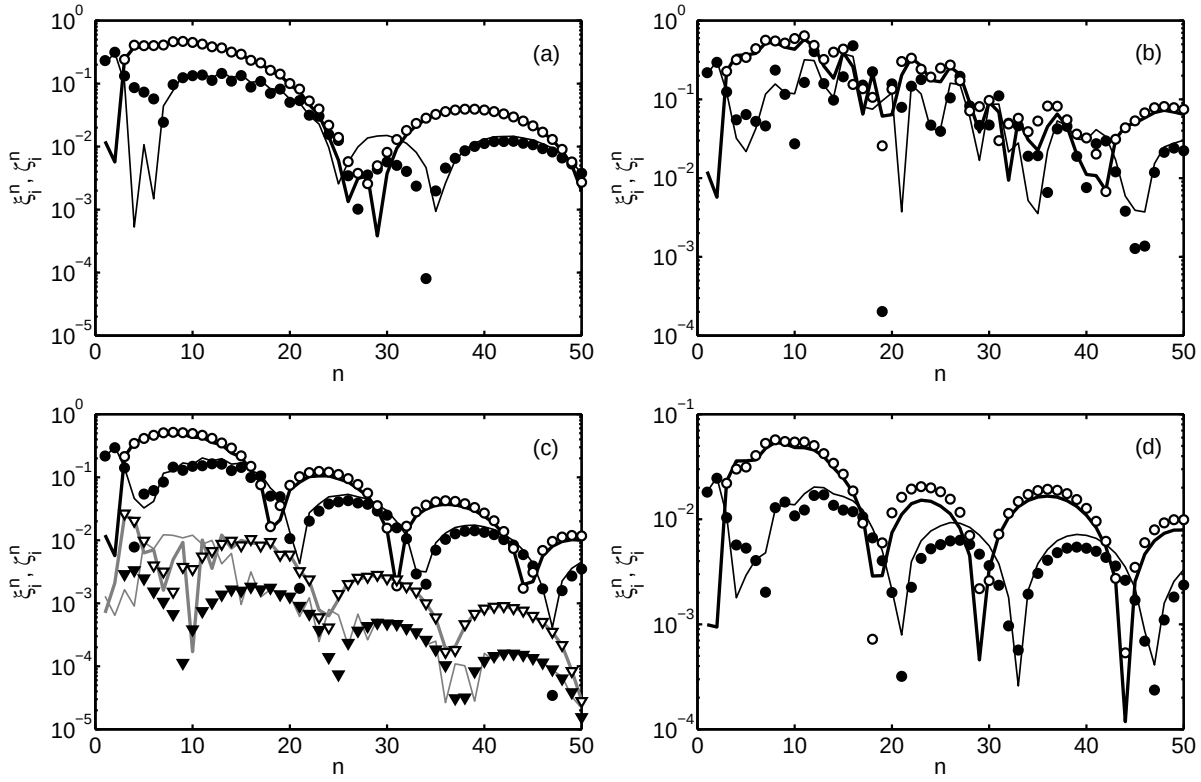

Figure 6. Modal amplitudes ξ_1^n (thin black line), ξ_2^n (thick black line), ξ_3^n (thin gray line), ξ_4^n (thick gray line) and their estimates $\tilde{\xi}_1^n$ (filled circles), $\tilde{\xi}_2^n$ (open circles), $\tilde{\xi}_3^n$ (filled triangles), $\tilde{\xi}_4^n$ (open triangles) during compensator control for $L = 1$ cm, $T = 205$ ms. (a) $x_o = 0.9$ cm and $m = 2$; (b) $x_o = 0.25$ cm and $m = 2$; (c) $x_o = 0.25$ cm and $m = 4$; (d) same as (b), but with smaller initial disturbance.

included in the truncation.

The nonlinear origin of the observer failure can be confirmed by reducing the initial deviation from the target state. For instance, replacing $\mathbf{z}_i \to \mathbf{z}_0 + (\mathbf{z}_i - \mathbf{z}_0)/10$ considerably improves the accuracy of the estimates as Fig. 6(d) illustrates. A partial solution to the problem is provided by increasing the truncation order of the compensator to include a number of weakly stable modes, in addition to the unstable ones. This has an effect of expanding the region of validity of the linear approximation (15). For instance, truncation to $m = 4$ modes produces radically more accurate estimates of the mode amplitudes (shown in Fig. 6(c)) for the same initial disturbance as in Figs. 6(a-b), mostly restoring the efficiency of the compensator. However, for $L \gtrsim 1.5$ cm the compensator fails for any truncation order, if the same electrode is used for pacing, control, and recording.

Although the range of parameters for which alternans can be suppressed is extended by replacing PIA with compensator control described here, even further improvement is possible with some modifications. While the maxima of $|f_i^u(x_c, \tau)|$ are achieved for the same value of τ regardless of the fiber length (this optimum is determined by the local cell dynamics), the maxima of $|e_i^u(x_o, \tau)|$ shift linearly with the fiber length (information propagates away from the pacing/control site with the speed given by the conduction velocity). For fibers longer than about 1 cm, controllability and observability may not be both satisfied by the same value of τ. For instance, for $L = 2$ cm, $|e_i^u(x_o, \tau)|$ are maximal for $\tau \approx T$ when $|f_i^u(x_p, \tau)|$ are near their minima (see Fig. 4), so that τ has to be chosen differently for the controller and the observer. If the system state is available and does not have to be reconstructed by an observer, feedback computed using model-based control can suppress alternans for up to $L \approx 2$ cm (see Fig. 1). For longer fibers the approach based on space- and time-localized current injections fails and *continuous*-time voltage measurement and current feedback are required to suppress alternans.

In summary, we have shown that following a systematic model-based approach it is possible to design a control procedure that overcomes the limitations of the PIA approach, yet is still simple to implement experimentally. The model-based analysis also allows one to determine how the electrodes should be arranged along the fiber, regardless of the method used to determine the feedback current. Specifically, the control electrodes should be placed at the spatial locations where the adjoint unstable eigenmodes are close to their maxima. This requirement can be satisfied, for instance, by collocating the pacing and control electrodes. Similarly, the recording electrodes should be placed where the unstable eigenmodes are near their maxima. For fibers shorter than 2 cm this can be achieved by plac-

ing one recording electrode near the opposite end of the fiber. For fibers longer than 2 cm an additional recording electrode is needed; it can be collocated with the pacing electrode. Furthermore, we explained that PIA control breaks down due to the loss of controllability when the second unstable mode appears. Finally, it should be mentioned that the analysis presented here is applicable to other excitable systems and, in particular, other types of cardiac tissue (e.g., atrial and ventricular muscle), paving the way for clinical applications.

Acknowledgements

This material is based upon work supported in part by the National Science Foundation under Grant No. 1028133. The authors are grateful to Flavio Fenton for many invaluable discussions.

References

Allexandre, D. and Otani, N. F. (2004) Preventing alternans induced spiral wave breakup in cardiac tissue: an ion channel based approach. *Phys. Rev. E*, **70**, pp. 061903.

Cherry, E. M. and Fenton, F. H. (2008). Visualization of spiral and scroll waves in simulated and experimental cardiac tissue. *New J. Phys.*, **10**, pp. 125016.

Christini, D. J. et al. (2006) Control of Alternans in Canine Cardiac Purkinje Fibers. *Phys. Rev. Lett.*, **96**, pp. 104101.

Echebarria, B. and Karma, A.(2002). Spatiotemporal control of cardiac alternans. *Chaos*, **12**, pp. 923.

Guevara, M. R. et al. (1984) Electrical alternans and period-doubling bifurcations. In *Comput. Cardiol.*, Park City, UT, USA, Sept. 18-20, pp. 167.

Hall, G. M. and Gauthier, D. J. (2002). Experimental control of cardiac muscle alternans. *Phys. Rev. Lett.*, **88**, pp. 198102.

Knoll, D. A. and Keyes, D. E. (2004) Jacobian-free Newton-Krylov methods: a survey of approaches and applications. *J. Comp. Phys.*, **193**, pp. 357.

Lehoucq, R. B. and Sorensen, D. C. (1996) Deflation Techniques for an Implicitly Re-Started Arnoldi Iteration. *SIAM J. Matr. Anal. Appl.*, **17**, pp. 789.

Mines, G. R. (1913). On dynamic equilibrium in the heart. *J. Physiol. (London)*, **46**(4-5), pp. 349–383.

Muñoz L. M., Stockton J. F. and Otani N. F. (2010). Applications of control theory to the dynamics and propagation of cardiac action potentials. *Annals Biomed. Eng.*, **38**, pp. 2865.

Noble, D. (1962) A modification of the Hodgkin-Huxley equations applicable to Purkinje fibre action and pacemaker potentials. *J. Physiol.*, **160**, pp. 317.

Pastore, J. M. et al. (1999). Mechanisim linking T-wave alternans to the genesis of cardiac fibrillation. *Circulation*, **99**, pp. 1385.

Pyragas, K. (1992) Continuous Control of Chaos by Self-Controlling Feedback. *Phys. Lett. A*, **170**, pp. 421.

Rappel, W. J., Fenton, F. H. and Karma, A. (1999) Spatiotemporal control of wave instabilities in cardiac tissue. *Phys. Rev. Lett.* **83**, pp. 456.

Watanabe, M. A. et al. (2001). Mechanisms for discordant alternans. *J. Cardiovasc. Electrophysiol.*, **12**, pp. 196

Zak, S. H. (2003) *Systems and Control*, Oxford University Press, New York.